IN-02-CR
128296
13P.

FLUCTUATIONS AND MASSIVE SEPARATION IN THREE-DIMENSIONAL SHOCK-WAVE/BOUNDARY-LAYER INTERACTIONS

M.I. Kussoy
Research Scientist, Eloret Institute

J.D. Brown
Research Associate, National Research Council

J.L. Brown, W.K. Lockman, and C.C. Horstman
Research Scientists, NASA Ames Research Center

NASA Ames Research Center, Moffett Field, California 94035, USA

INTRODUCTION

Shock-wave unsteadiness has long been observed in rapidly compressed supersonic turbulent boundary-layer flows with significant separation.[1] The shock oscillations are characterized by large time scales, relative to those associated with the turbulence in the upstream, undisturbed boundary layer, and have been identified with low frequency, large amplitude (again, relative to the upstream boundary layer), wall-pressure fluctuations.[2,3] Researchers have been interested in these flows for some time because of direct aerodynamic and turbo-machinery applications. However, until recently, most experiments reported long-time-averaged data without addressing the unsteady aspects. This was often due to a lack of the necessary instrumentation.

In the last few years, the advent of miniaturized high-frequency pressure transducers, and the continued development of the laser Doppler velocimeter (LDV), which non-intrusively measures velocity, have given new, timely, facility to the study of shock-wave unsteadiness as it relates to boundary-layer behavior. This comes as demands for more detailed information on separated shock boundary-layer interactions have been generated by expanding efforts in computational fluid dynamics (CFD). To date, computations have been successful in predicting a limited class of such interactions,[4,5] principally 2-D flows, and 3-D flows in which the shock waves were planar. The same combinations of numerics and turbulence models have as yet failed to predict a whole other group of separated flows, to be discussed here, with *non*-planar shocks.[6,7] This failure, coupled with knowledge that the turbulence models employed do not provide for the shock unsteadiness which is observed experimentally, has produced interest in the effect that unsteadiness has on the separating boundary layer.

Certain basic questions have been raised. First, can the effects of the unsteadiness be removed from the mean experimental data by some conditional sampling technique, so that "snapshots" of the flow, corresponding to specific shock positions (or phase angles), can be extracted and studied independently? Second, are the measured turbulence quantities for flows with large separation zones dominated by some "pseudo-turbulence" which results from the overall bimodal nature (shock forward - shock back) of the interaction? Third, does it really matter? Can the unsampled time-averaged data be meaningfully compared to the computations, ignoring the fact that the shock wave is unsteady? If not, can a shock unsteadiness model be developed that would improve the predictive accuracy of current computational schemes?

In recent years, a joint experimental and computational program aimed at addressing some of these questions has been in progress at the NASA Ames Research Center. A Mach 2.85 shock-wave/turbulent boundary-layer flow was set up over a series of cylinder-flare bodies in the High Reynolds Number Channel 1. In the first phase of this investigation, the transition from fully attached to fully separated flow was stud-

ied using axisymmetric flares with increasing (12.5°–30°) compression angles.[8,9] In the second phase, the 30° flare was inclined relative to the cylinder axis, so that the effect on a separated flow of increasing 3-dimensionality could be observed.[6,7] For each of the separated cases investigated in phases 1 and 2, shock unsteadiness was discussed, but no attempt was made to remove its effect from the reported mean data.

The current paper examines in some detail two 3-D separated cases. A simple conditional sampling technique is applied to the data to group them according to an associated shock position. Mean velocities and turbulent kinetic energies, computed from the conditionally sampled data, are compared to those from the unsorted data and to computed values. (The predictions are included to inform the reader as to the present state of the art. They do not represent any previously unpublished developments in CFD.) Finally, of the "basic questions" raised above, the first three are addressed. Namely, 1) can conditional sampling be used to provide "snapshots" of the flow; 2) are averaged turbulence quantities dominated by the bimodal nature of the interaction; and 3) is the shock unsteadiness really important to computational accuracy.

DETAILS OF THE EXPERIMENT

Complete details of the experimental setup and procedures have been previously reported.[6] A summary of the relevant aspects follows.

The experiment was performed in a 25.4-by-38.1 cm rectangular test section of Ames Research Center's High Reynolds Number Channel-I. This air-charged blowdown tunnel employs interchangeable nozzles and test sections to generate a range of transonic and supersonic Mach numbers.

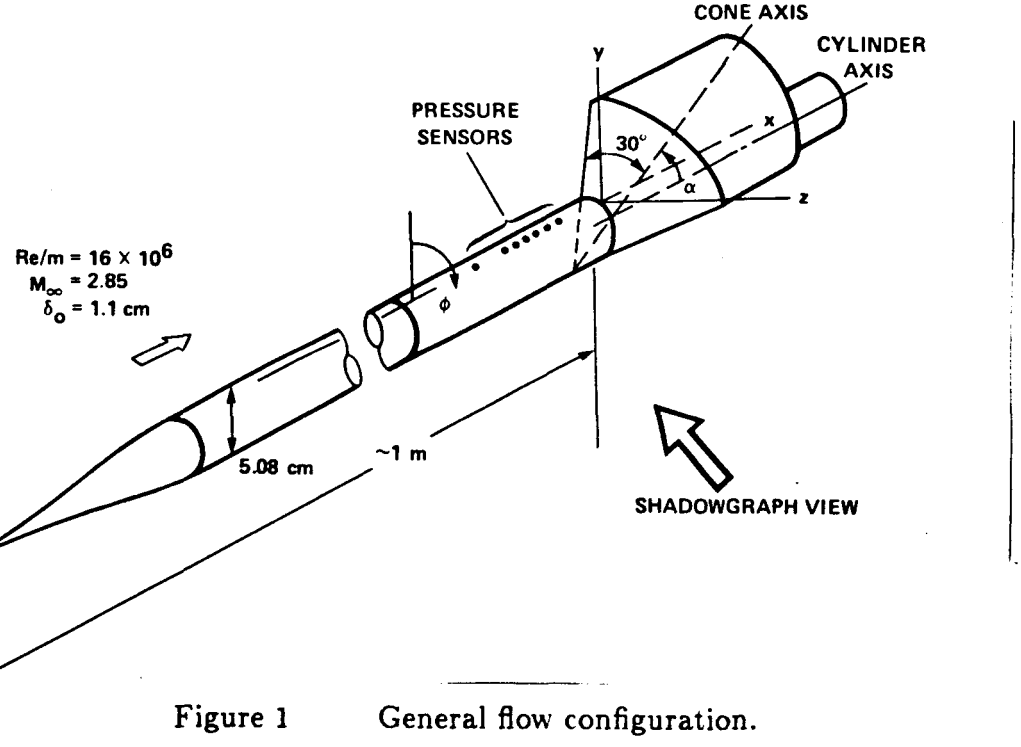

Figure 1 General flow configuration.

Figure 1 shows the basic flow configuration, and the associated coordinate system used in the data analysis. An axisymmetric, equilibrium turbulent boundary layer forms over the 5.08-cm-diam stainless steel cylinder which is aligned with the tunnel axis. The cusped nose prevents formation of strong shocks that might otherwise reflect off tunnel walls back to the cylinder. The flow is abruptly compressed as it approaches the 30° half-angle flare, and the boundary layer then separates from the cylinder. For nonzero flare-inclination angles (α), the interaction is three dimensional.

The principal region of study extended approximately five undisturbed boundary-layer thicknesses, δ_0, upstream of the compression corner, and a similar distance downstream along the flare. This paper discusses two 3-D configurations, $\alpha = 5°$ and 23°. The data presented are for the upper symmetry plane, $z = \phi = 0$, only.

Nominal total and undisturbed flow conditions were: $T_t = 270°\text{K}$, $p_t = 1.7$ atm, $M_\infty = 2.85$, $Re = 16 \times 10^6/\text{m}$, and $\delta_0 = 1.1$ cm.

Velocity measurements were made using a two-component laser Doppler velocimeter (LDV) operating in the forward scatter mode. The system employed a 4-W argon-ion laser, signal-processor counters, Bragg cells for frequency shifting, and half-micron latex light-scattering particles. Two-color operation of the LDV was used to distinguish the individual velocity components, while directional discrimination for each component was achieved with frequency shifting. Reference 6 gives details of the system components, and the procedures for alignment, calibration, and operation. A PDP 11/34 minicomputer was used for data acquisition and initial analysis. To increase speed, the data were stored on hard disk during tunnel runs. They were later transferred to magnetic tape for reduction, and then to a VAX 11/785 computer for all subsequent analyses.

The cylinder portion of the model was instrumented with six high-speed pressure transducers (DC to 100 KHz) mounted just below the surface, and spaced 0.5 cm apart along the $\phi = 0°$ surface line. They were used during LDV data acquisition to record instantaneous wall pressures in the vicinity of the separation shock.

DETAILS OF COMPUTATIONS

The equations used to describe the mean flow were the time dependent, Reynolds-averaged Navier-Stokes equations for a 3-D fluid. For turbulence closure, the two equation, k-ϵ eddy-viscosity model[10] with wall-function boundary conditions[4] was used. The MacCormack explicit, second order, predictor corrector, finite-volume numerical procedure[11] was employed.

The computational domain consisted of uniform mesh spacing in the streamwise (x) and azimuthal (ϕ) directions. In the vertical (y) direction, a geometrically stretched spacing was used near the solid surfaces, followed by a uniform spacing. The total mesh size was 64 points in the streamwise direction, 33 in the vertical direction, and 38 in the azimuthal. Typically, 16 mesh points were used to resolve the boundary layer.

The upstream boundary conditions were prescribed by a combination of uniform free-stream conditions and the results of a boundary-layer computation matching the experimental displacement thickness. At the downstream boundary, the gradients of the flow variables in the streamwise direction were set to zero. In the azimuthal direction, symmetry conditions were applied at $\phi = 0°$ and $\phi = 180°$. No-slip and constant wall temperature conditions were imposed at the surface where turbulent kinetic energy and dissipation were set to zero. Free-stream conditions were applied at the outer boundary.

To reduce the time required to achieve a converged solution, wall-function boundary conditions were used at the cylinder and flare surfaces. The compressible two-dimensional wall functions derived in ref. 4 were extended to 3-D flows by replacing the horizontal velocity with the total velocity parallel to the wall. The flow direction was also assumed to remain constant between the surface and the first grid point away from the surface. The y^+ location of the first grid point varied from 30 to 120.

CONDITIONAL SAMPLING

To examine the effects of shock unsteadiness on the time-averaged data, such as velocities and turbulent stresses, it was desired to construct different ensembles of instanta-

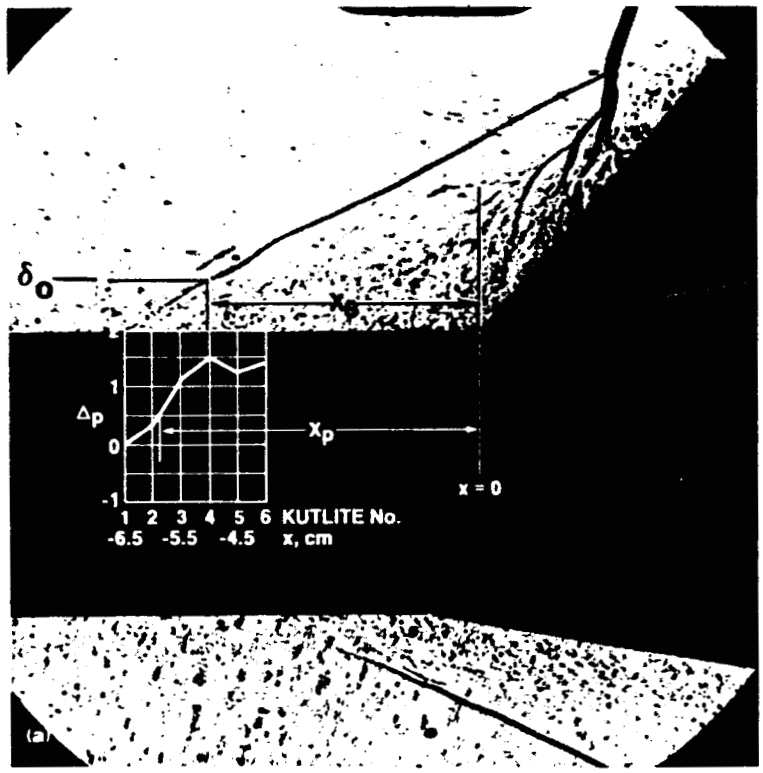

a) Shock forward.

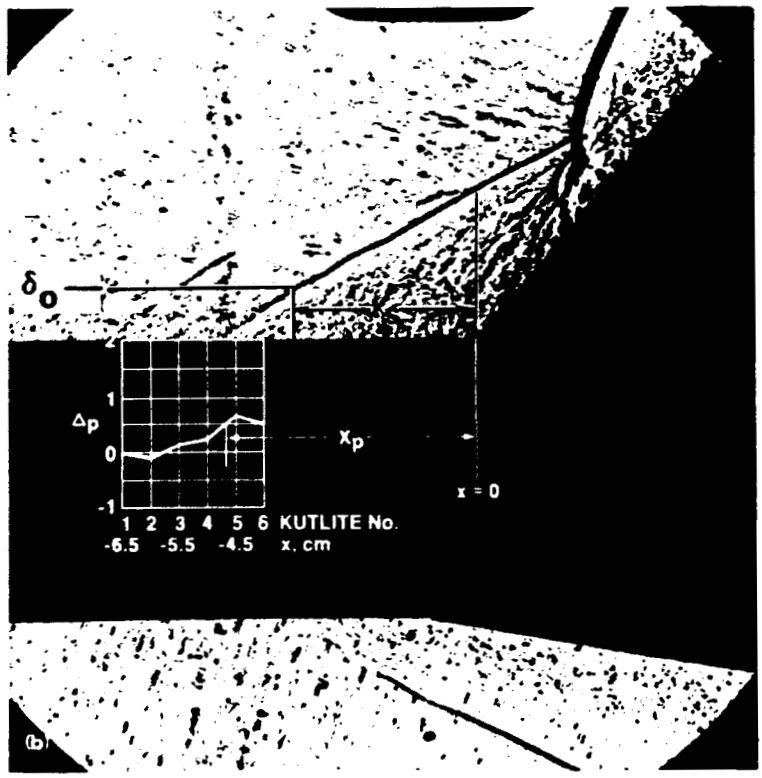

b) Shock back.

Figure 2 Shadowgraph and related instantaneous surface pressures.

neous measurements, each corresponding to a particular shock wave position (or phase angle). Then, by comparing the mean flow quantities derived from these ensembles with each other, and with those derived from the ensemble which embodied all shock positions, the response to changes in shock location could be observed.

To accomplish this, it was necessary to conditionally sample, and sort, the instantaneous LDV measurements according to the position (or region) the shock was in when they were acquired. This could be done during data acquisition itself by employing a trigger that, based on a pre-set condition, would have the LDV selectively take data. However, it was judged a more practical approach to conditionally sample during post-test analysis of the measurements that were made unconditionally, i.e., whenever a valid LDV event was registered. This required large numbers of data to be taken so that each sorted ensemble was large enough to yield statistically valid mean results. The question of how to link individual data with corresponding shock positions also had to be answered.

Figure 2 illustrates the experimental procedure used to relate the shock movement to surface pressures. Simultaneous measurements were taken of the shock wave motion (with high speed—9000 frames/sec—shadowgraph movies) and surface pressures at 6 axial locations 0.5 cm apart (using high frequency miniaturized transducers). Computer generated timing marks were recorded on the film when surface pressures were sampled, and the result was that for each film frame there was an associated instantaneous pressure distribution. The figure shows a high speed shadowgraph frame and its related pressure distribution for a "shock forward" and a "shock back" case. Differential pressure transducers were used, and the values shown represent changes from the undisturbed wall pressure.

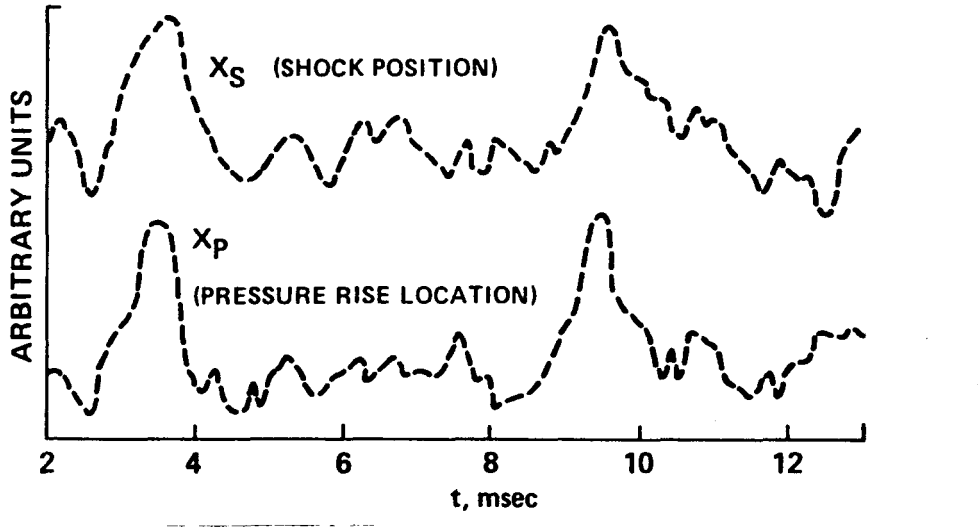

Figure 3 Correlation of shock position with surface pressure.

Figure 2 also illustrates the definitions of X_s, the streamwise distance from the corner to where the shock intersects the boundary layer edge, and X_p, to where the differential pressure crosses a value of 0.5. The variations of X_s and X_p with time, for a typical 60 msec interval, are shown in figure 3. The high degree of correlation between these two quantities—they differ, for the most part, by a constant—indicates that shock location can be deduced, with reasonable accuracy and relative ease, from surface pressure measurements.

All LDV data were measured and recorded simultaneously with the pressures obtained from the array of transducers. Numerous criteria, applied to the pressures, were considered for conditional sampling of the instantaneous velocities. However, for the present report, one of the simpler algorithms was chosen.

For each LDV measurement location, the overall mean and standard deviation of the pressure ($\bar{p}$ and p'_{rms}) were computed from the transducer which was positioned beneath the average shock position, as determined visually from shadowgraph movies. Then, the instantaneous pressure levels ($p(t)$) were examined at that transducer, and, based on them, the corresponding velocity pairs ($u(t)$, $v(t)$) were selected for, or ex-

cluded from, conditionally-sampled ensembles. This paper identifies a "shock forward" (SF) case which includes all velocity pairs for which $p(t) \geq \overline{p} + p'_{rms}$ at the surface location beneath the mean shock position. It also presents a "shock back" (SB) case for which velocities correspond to $p(t) \leq \overline{p} - .5p'_{rms}$. Finally, the flow quantities derived from the full data ensemble with no conditions applied, constitute the "all data" (AD) case. The coefficient of 0.5 in the SB criterion was necessary to retain a sufficient number of data to yield reliable statistics. The nature of the distribution of pressure levels is such that the number of measurements corresponding to SB drops rapidly as that coefficient is lowered below -0.5.

RESULTS AND DISCUSSION

Figure 4 shows mean streamlines for the SF, SB, AD, and computed cases of $\alpha = 5°$. Figure 5 presents the same information for $\alpha = 23°$. The streamlines are constructed from the appropriate ensemble-averaged velocity ($\overline{u}$ and $\overline{v}$) field using a 4-point spatial interpolation, predictor-corrector scheme. As the computations predict flows that are completely steady, the corresponding streamlines also represent streaklines and particle paths. The sharp turns near the surface of the flare in the 5° streamlines reflect a scarcity of data in that region. The double core in the 23° AD case was observed to disappear when a small change in vertical velocity was imposed, and is not thought to accurately represent the flow. The authors believe that the overall smoothness of the streamlines, when no special measures were taken to achieve it, indicates the data to be of high quality.

A significant point to be made from these figures is that in the experiment, there is little, if any change in the appearance of the mean velocity field as the shock wave fluctuates between its upstream and downstream positions. The recirculation core (that point, or region, shown by a confluence of streamlines, from which the flow exits the symmetry plane) moves back and forth along the cylinder. Its strength seems to vary also, with more of the surrounding fluid affected in the shock forward case than in the shock back. However, the overall form of the flow apparently does not change.

The computations, on the other hand, depict a flow that is significantly different from any of the measured cases for either flare angle. The predicted recirculation zone is larger than even that shown in the SF case, with the particles apparently spiraling inward much more slowly toward a core which is located well up along the flare rather than over the cylinder.

In figures 6 and 7, contours of the mean streamwise velocity are shown for the separated regions of $\alpha = 5°$ and $\alpha = 23°$ respectively. Only experimental results (SF, SB, and AD) are given. The contours show the separation "bubble" to expand and contract like a ballon (rather than translating up- and downstream, for example) as the shock position varies. Relative to the motion of the boundary-layer separation point (approximated as where the $\overline{u} = 0$ contour is nearest the cylinder, and marked "S"), reattachment ($\overline{u} = 0$ nearest the flare, marked "R") seems to vary far less, from SF to SB, for $\alpha = 23°$ than for $\alpha = 5°$. This may be another indication of the protuberance-like character of the 23° flare which was discussed previously in some detail.[6]

Figures 8 and 9 show the streamwise distributions (SF, SB, AD, and computations) of the maximum turbulent kinetic energy (k_{max}) for the two flare angles studied. It is noted that the experimental kinetic energies are from 2-component velocity data, and the assumption has been made that the third normal stress, w'_{rms} is equal to the average of the two that were measured.

For $\alpha = 5°$, it is almost uniformly true that k_{max} for the SF case is larger than k_{max} for AD at a given location. The SB value is consistently the lowest. The reasons for this are presently unknown, but the digitization of high-speed shadowgraph movies, and the computer simulation of a moving shock wave are being used to search for clues.

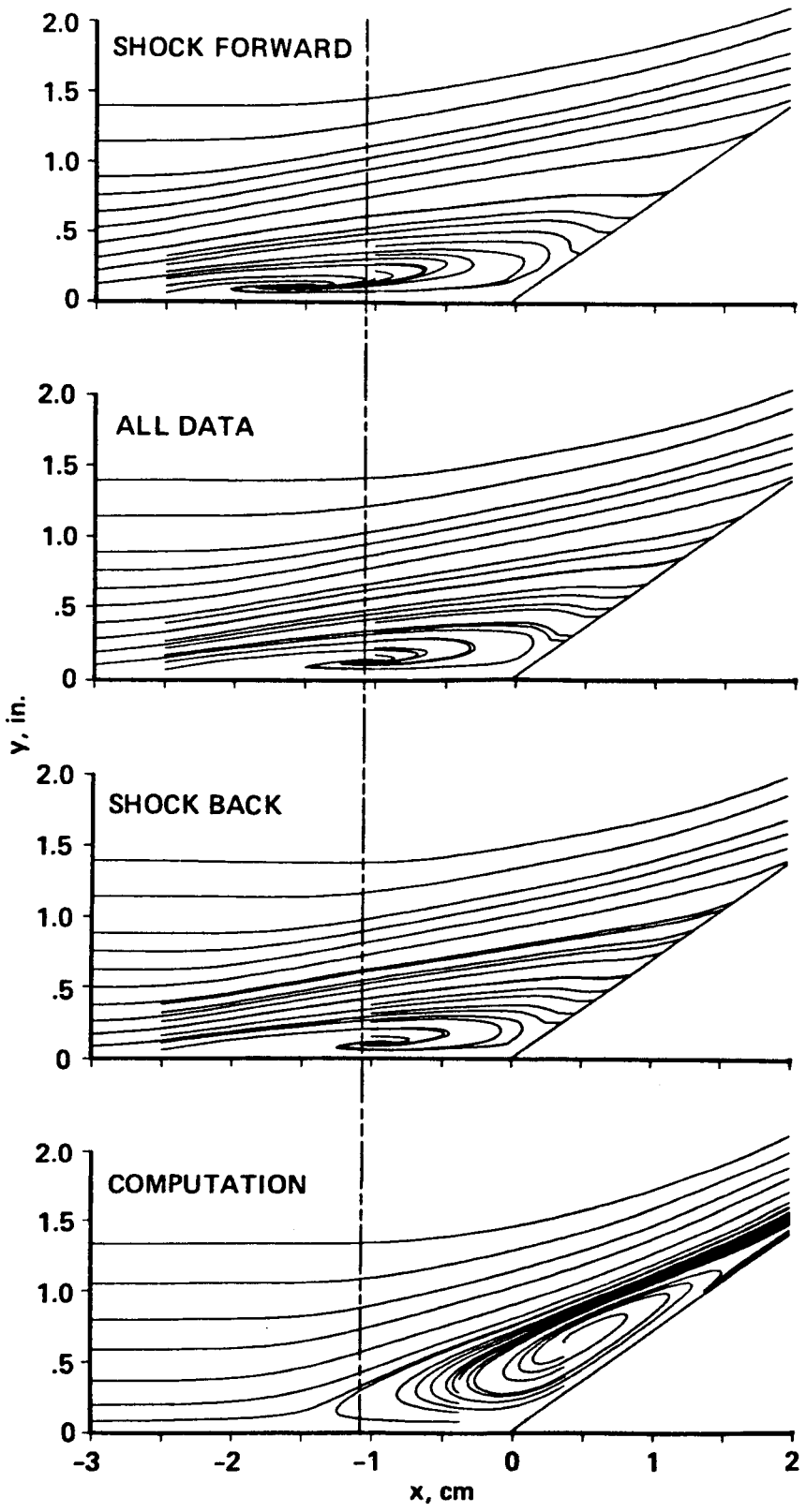

Figure 4 Mean streamlines, $\alpha = 5°$, $\phi = 0°$.

The fact that k_{max} for the AD case exceeds the SF value at $x = -3$ cm, is due to strong influence from the shock motion. The distribution of velocities at this point exhibits two distinct states, such as S_1 and S_2 in the joint probability density diagram shown in fig. 10. Each state can be assigned its own probability of occurrence, P_1 and P_2, along with values for mean velocities and turbulent stresses (i.e., $\overline{u_1}$, $v_{2_{rms}}'$, etc.).

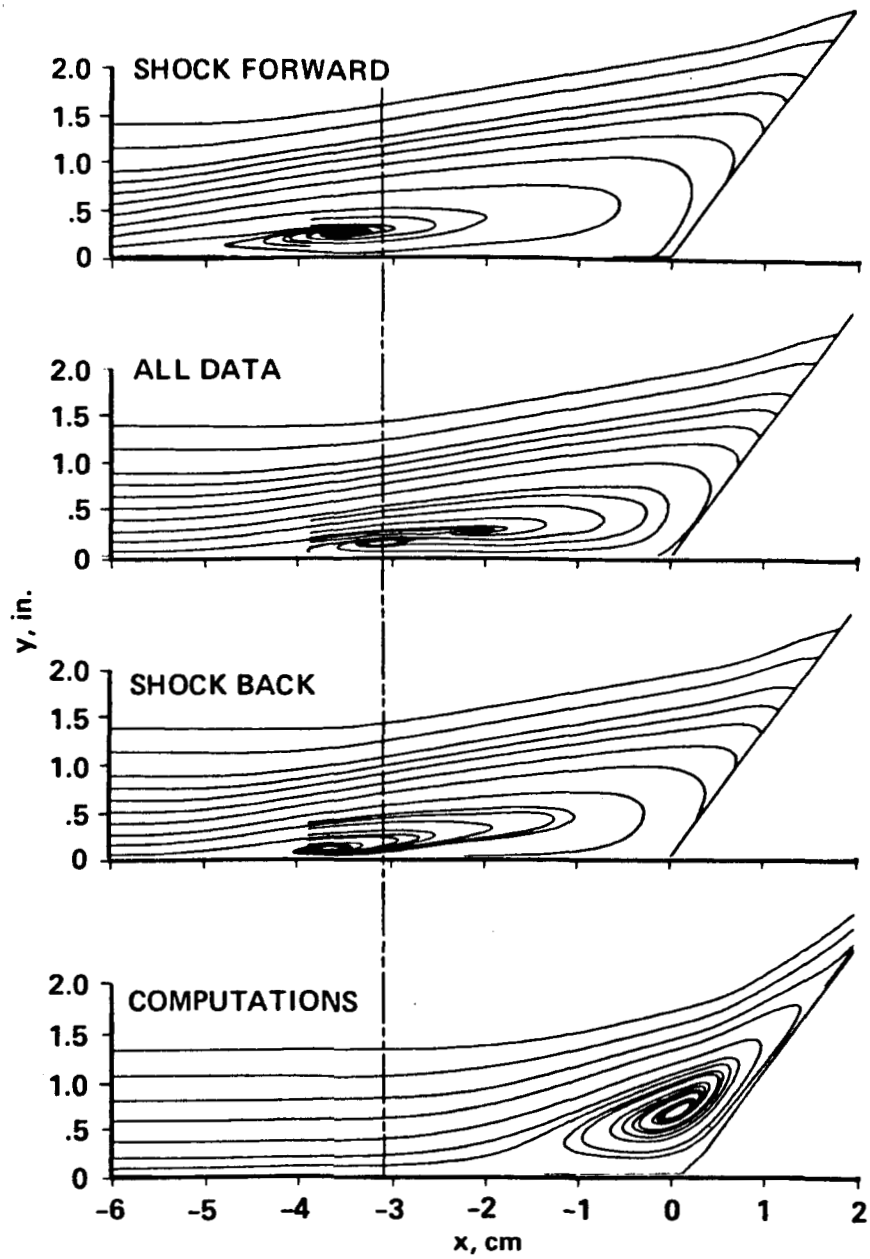

Figure 5 Mean streamlines, $\alpha = 23°$, $\phi = 0°$.

Reference 7 asserts that the turbulent kinetic energy of the all-data case is not merely a weighted (by P) sum of the energies for the two states which comprise it, but is also a function of the difference between the states and the product of their probabilities. This "organized" or "coherent" (as opposed to dissipative) contribution to the turbulent kinetic energy is expressed by $P_1 P_2((\overline{u_1} - \overline{u_2})^2 + (\overline{v_1} - \overline{v_2})^2)$. It is clearly significant in the immediate vicinity of the shock, where histograms such as that shown in fig. 10 are common, but its importance appears to fall off rapidly away from the shock.

The distribution of k_{max} for $\alpha = 23°$ (fig. 9) is more complicated than for 5°. The AD levels remain higher than those for SF from $x = -5.8$ cm to $x = -0.3$ cm. This may result from larger amplitude shock oscillations, and a more persistent "coherent" contribution. However, for much of this same span, the SF levels stay at or below those for the SB case. The trends for the 5° flare are closely matched by those observed for $\alpha = 0°$ and 10° (though the latter two are not shown), and once again the 23° flow demonstrates significantly different behavior than for flows over lesser inclined flares.

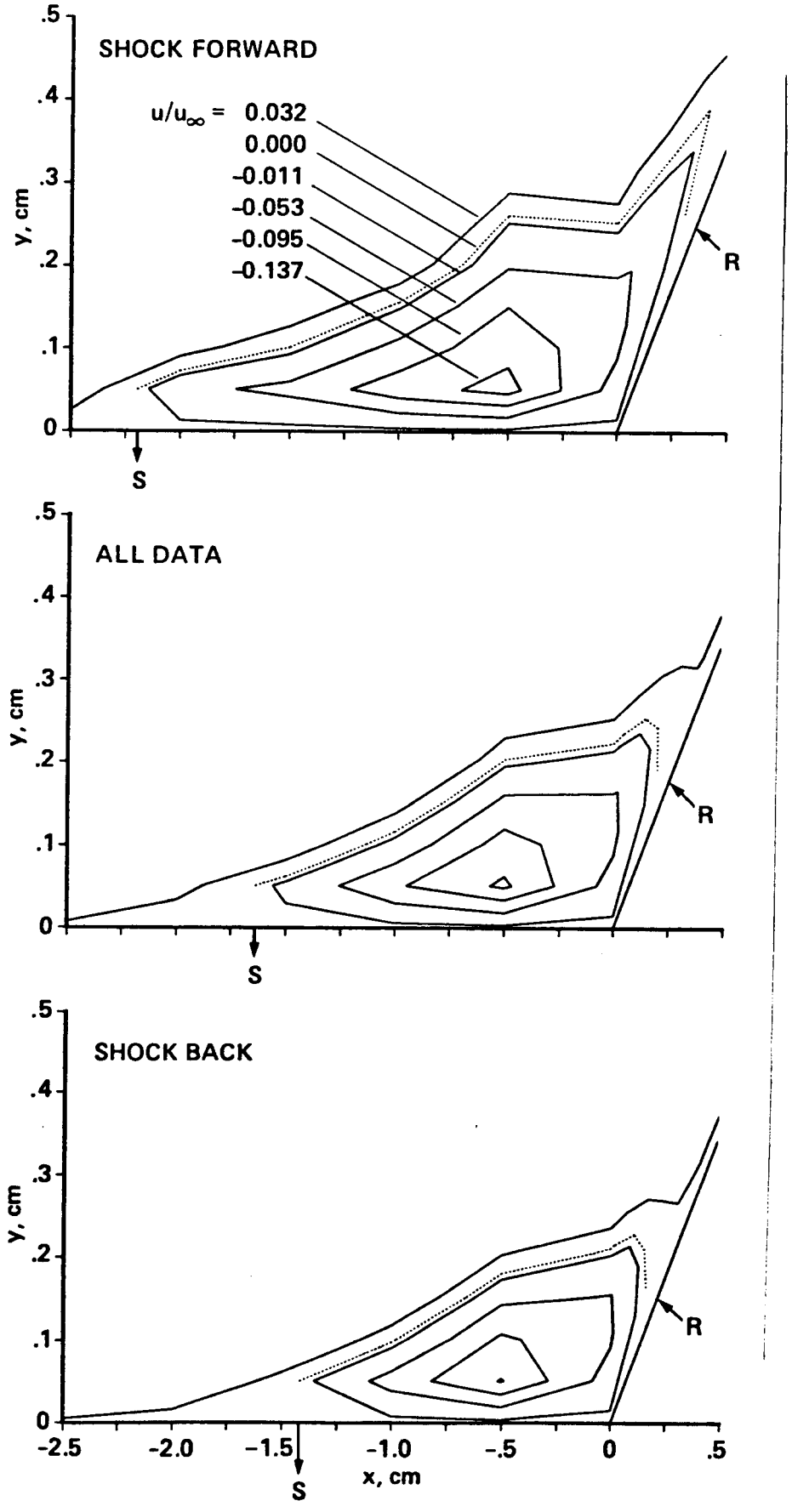

Figure 6 Mean velocity contours in separated flow region, experiment only, $\alpha = 5°$, $\phi = 0°$.

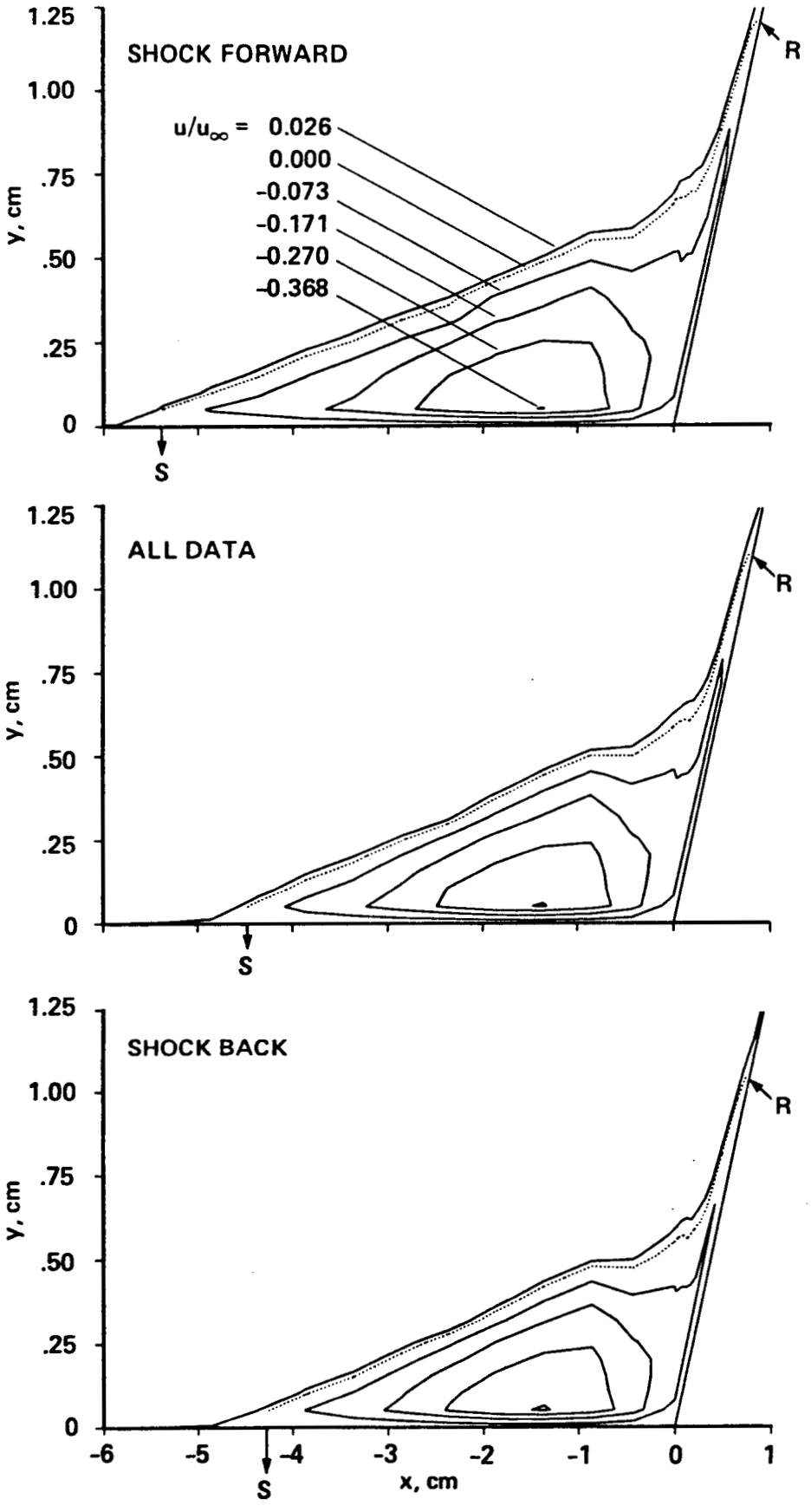

Figure 7 Mean velocity contours in separated flow region, experiment only, $\alpha = 23°$, $\phi = 0°$.

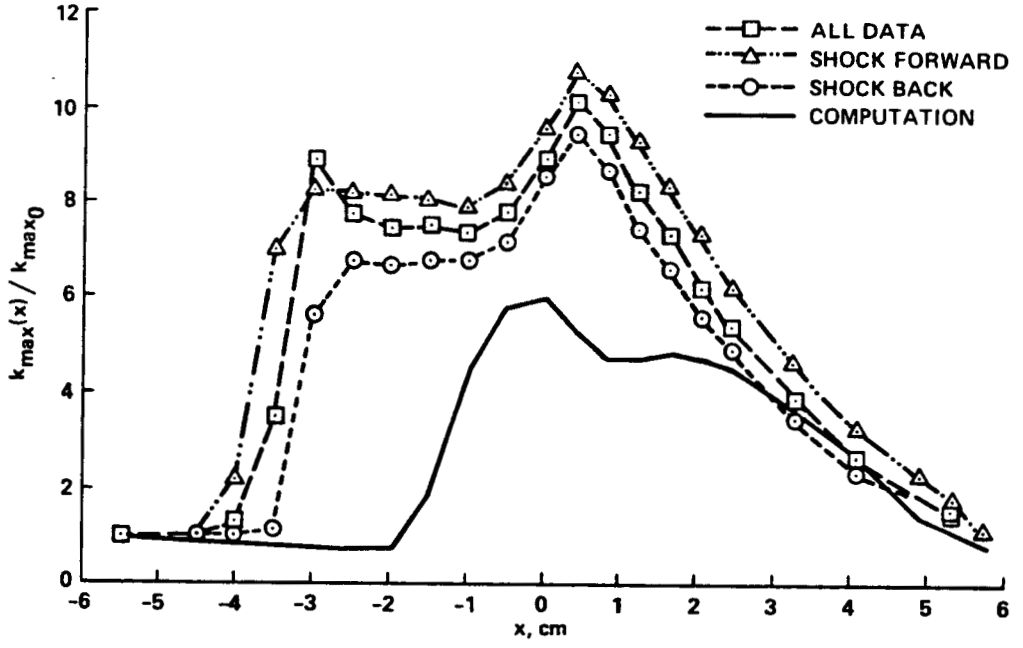

Figure 8 Distribution in x of maximum (2D) turbulent kinetic energy, $\alpha = 5°$, $\phi = 0°$.

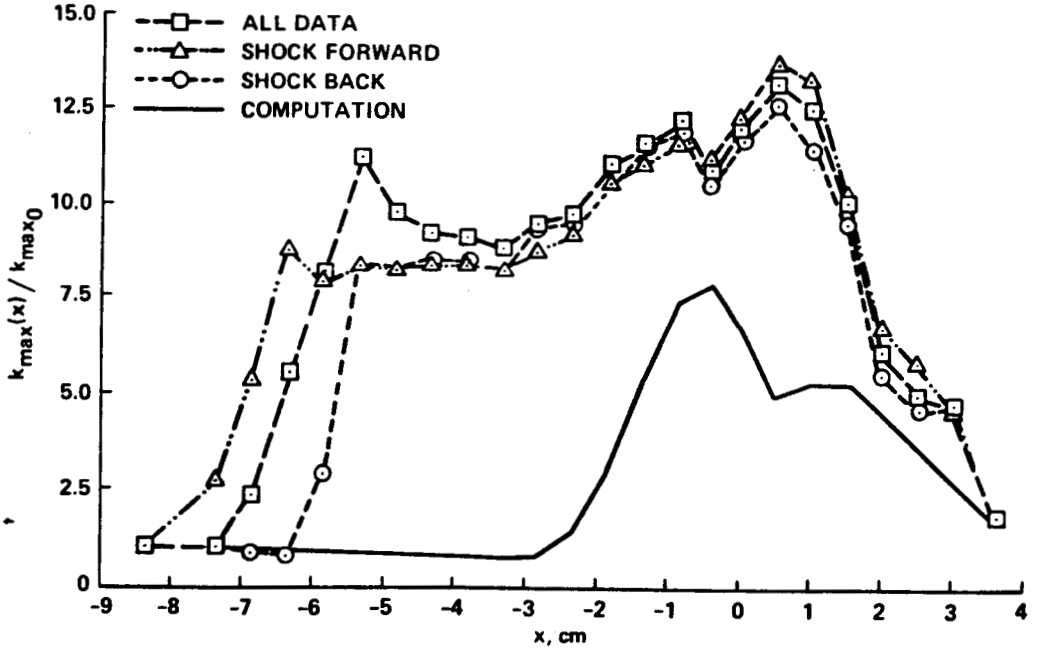

Figure 9 Distribution in x of maximum (2D) turbulent kinetic energy, $\alpha = 23°$, $\phi = 0°$.

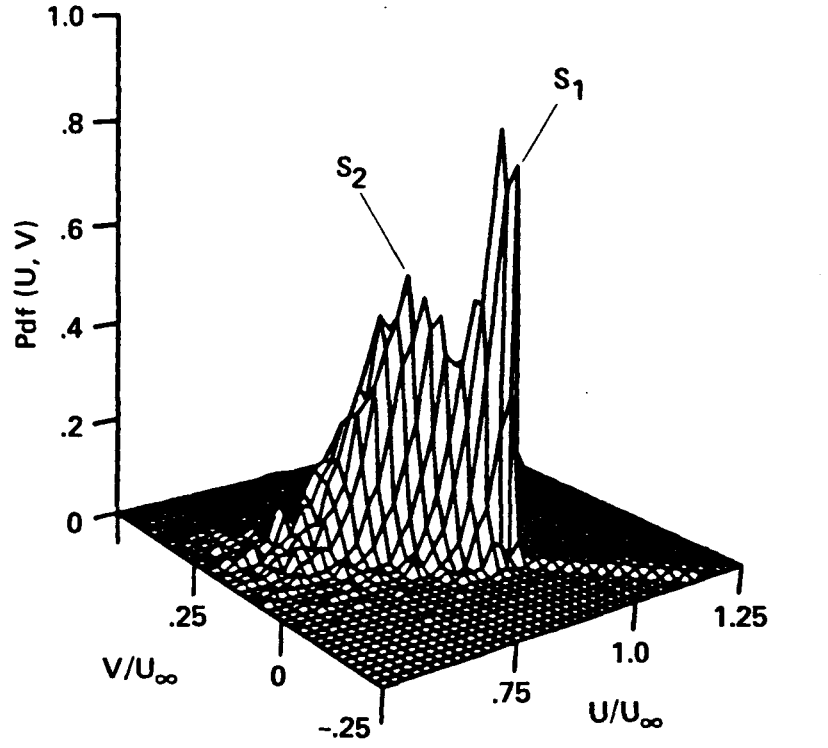

Figure 10 Joint probability density diagram from LDV data, $\phi = 0°$, $\alpha = 5°$, $x = 3$ cm.

Finally, the computed k_{max} distributions bear little or no resemblance to those measured, whether conditionally sampled or not. Even when compared to the SB case, for both flares, the initial rise in computed turbulent energy occurs far downstream of where it is actually measured. The absolute peak k levels in the computations are well below 60% of those measured, and they also occur at different x-locations.

CONCLUSIONS

The authors have studied numerous two- and three-dimensional shock-wave turbulent boundary-layer interactions at Mach 2.85. This paper has presented results for two fully separated flows, one moderately three dimensional, and the other highly so. The analysis focussed on the large scale unsteadiness of the separation shock wave (which has long been observed in this class of flows) as it relates to time-averaged flow quantities such as mean velocities and turbulent stresses. To do so, a basic technique was employed to conditionally sample flow-field measurements using an instantaneous wall pressure level, and statistics calculated from the resulting sorted ensembles were compared with those derived from the unsampled data, and with computed (Navier-Stokes) results. Some basic questions, outlined in the introduction, have been addressed.

Regarding the ability to remove unsteadiness effects through conditional sampling: The coupling of high speed shadowgraph and surface-pressure data indicated that the latter could be used to infer shock position. The performance herein of a relatively simple conditional sampling scheme which uses an instantaneous pressure level to sort velocity data, suggests that "snapshots" of the flow corresponding to specific shock positions *can* be obtained. This, however, does not remove all unsteadiness effects, since the many fluid particles whose velocities comprise those snapshots still were influenced by an unsteady shock wave.

On the subject of "pseudo-turbulence": It is possible that for the $\alpha = 23°$ case, which is highly three dimensional, turbulence quantities are dominated by a "coherent" contribution from the shock motion throughout much of the flow. For the lesser inclined flare, any such effect seems to be limited to the immediate vicinity of the shock, the only place where the all-data case shows higher turbulence levels than the sorted shock-forward (SF) case.

Finally, on the issue of how important the shock unsteadiness is to the accuracy of the computations, the following points should be considered. As the shock moves forward, the reverse flow region seems to expand, pushing the separation point forward along the cylinder, the reattachment point aft along the flare, and the zero velocity line outward from the corner. The region contracts in a similar fashion as the shock retreats. Still, the basic character of the mean flow-field, identified by a recirculation core located over the cylinder, does not change with shock position. However, the computations predict a completely steady flow, with the recirculation core above the flare, that does not approximate that basic character. This gives cause to wonder whether any improvement in computational accuracy would be realized simply by the addition of an unsteady shock wave mechanism.

REFERENCES

1 Bogdonoff, S. M., Some Experimental Studies of the Separation of Supersonic Turbulent Boundary Layers, Aeronautical Engineering Department, Princeton University, Report 336, June 1955.

2 Dolling, D. S. and Bogdonoff, S. M., An Experimental Investigation of the Unsteady Behavior of Blunt Fin-Induced Shock Wave Turbulent Boundary Layer Interactions, AIAA Paper 81-1287, 1981.

3 Dolling, D. S. and Brusniak, L., Separation Shock Motion in Fin, Cylinder and Compression Ramp-Induced Turbulent Interactions, AIAA Paper 87–1368, 1987.

4 Viegas, J. R., Rubesin, M. W., and Horstman, C. C., On the Use of Wall Functions as Boundary Conditions for Two-Dimensional Separated Compressible Flows, AIAA Paper 85-0180, 1985.

5 Knight, D., Horstman, C. C., Ruderich, R., Mao, M. -F., and Bogdonoff, S., Supersonic Turbulent Flow Past a 3-D Swept Compression Corner at Mach 3, AIAA Paper 87–0551, 1987.

6 Brown, J. D., Two-Component LDV Investigation of Shock-Related Turbulent Boundary Layer Separation with Increasing Three Dimensionality, Ph.D. Thesis, University of California, Berkeley, 1986.

7 Brown, J. D., Brown J. L., Kussoy, M. I., Holt, M., and Horstman, C. C., Two-Component LDV Investigation of 3-Dimensional Shock/Turbulent Boundary Layer Interactions, AIAA Paper 87–0553, 1987.

8 Brown, J. L., Kussoy, M. I., and Coakley, T. J., Turbulent Properties of Axisymmetric Shock-Wave Boundary-Layer Interaction Flows, IUTAM Symposium, Paris, France, 1985.

9 Dunnagan, S. E., Brown, J. L., and Miles, J. B., Holographic Interferometry Study of an Axisymmetric Shock-Wave Boundary-Layer Strong Interaction Flow, *AIAA Journal*, Vol. 25, No. 2, pp. 294–299, Feb. 1987.

10 Jones, W. P. and Launder, B. E., The Prediction of Laminarization with a Two-Equation Model of Turbulence, *Int. Journal of Heat and Mass Transfer*, Vol. 15, pp. 301–314, Feb. 1972.

11 MacCormack, R. W., Numerical Solution of the Interaction of a Shock Wave with a Laminar Boundary Layer, *Lecture Notes in Physics*, Vol. 8, 1972, Springer-Verlag, Berlin, pp. 151–163.